International Journal of Heat and Mass Transfer 52 (2009) 5661–5674

Contents lists available at ScienceDirect

International Journal of Heat and Mass Transfer

journal homepage: www.elsevier.com/locate/ijhmt

Ledinegg instability in microchannels

Tiejun Zhang [a,d], Tao Tong [b], Je-Young Chang [c], Yoav Peles [d,*], Ravi Prasher [e,*], Michael K. Jensen [d], John T. Wen [f], Patrick Phelan [e]

[a] Center for Automation Technologies and Systems, Rensselaer Polytechnic Institute, 110 8th Street, Troy, NY 12180, USA
[b] Department of Mechanical Engineering, University of California, Berkeley, CA 94720, USA
[c] Intel Corporation, 5000 W. Chandler Blvd. Chandler, AZ 85226, USA
[d] Department of Mechanical, Aerospace & Nuclear Engineering, Rensselaer Polytechnic Institute, 110 8th Street, Troy, NY 12180, USA
[e] Department of Mechanical and Aerospace Engineering, Arizona State University Tempe, AZ 85287, USA
[f] Department of Electrical, Computer and System Engineering, Rensselaer Polytechnic Institute, 110 8th Street, Troy, NY 12180, USA

ARTICLE INFO

Article history:
Received 21 April 2009
Received in revised form 3 September 2009
Available online 30 September 2009

Keywords:
Boiling
Microchannel
Two-phase flow
Flow instability

ABSTRACT

The static Ledinegg instability in horizontal microchannels under different flow conditions and fluids pertinent to electronics cooling was studied experimentally and numerically. Two fluids, water at sub-atmospheric pressures and refrigerant HFE-7100, were examined for a range of heat fluxes, mass fluxes, and channel hydraulic diameters. Numerical predictions from the developed pressure gradient model agree well with results from the flow boiling experiments. The model was used to quantify the susceptibility of the system to the Ledinegg instability. A parametric instability study was systematically conducted with varying system pressure, heat flux, inlet subcooling, and channel size with and without inlet restrictor. Increasing system pressure and channel diameter, reducing parallel channel number and channel length, and including an inlet restrictor can enhance the flow stability in microchannels.

1. Introduction

Flow boiling instabilities have been a cause for great concern in the design of conventional scale heat exchangers. The deleterious effects of these phenomena on conventional systems are well documented and have been aggressively researched since the early 1960s [1]. Flow boiling oscillations modify the hydrodynamics of the flow, introduce severe structural vibrations, generate acoustic noise, and can jeopardize the structural integrity of the system. But, most importantly, flow oscillations can lead to the premature initiation of the critical heat flux condition [2–4], which, in turn, will result in a very ineffective heat transfer process; for heat flux controlled systems, elevated surface temperatures and possible complete destruction of the devices (burnout) may occur.

Studies performed in the last decade by several independent groups [5–12] strongly suggest that at the micro scale the phenomenon can be more noticeable than at the macro scale. These studies identified several flow boiling instability modes in microchannels, including rapid bubble growth, parallel channel instability, and upstream compressible flow instability. The parallel channel instability is closely related to a well acknowledged and important static instability termed the flow excursion (or Ledinegg) instability. While a single instability mode can be activated independently of other modes, several modes can also be interlinked. For instance, the rapid bubble growth instability can trigger early manifestation of the parallel channel instability, which can cause early transition to the critical heat flux condition [13].

By increasing the system pressure for flow boiling of water in microchannels, Kuo and Peles [14] have shown that the resulting decrease in the liquid-to-vapor density ratio, ρ_l/ρ_v, causes flow instabilities to diminish. The reduction of the negative slope of the pressure drop–mass flux curve of the two-phase mixture at low ρ_l/ρ_v weakened the system's susceptibility to the instability, resulting in a much stabilized flow. This, in turn, mitigated the premature critical heat flux condition induced by flow oscillations and significantly increased the corresponding maximum heat flux attainable of the system at elevated pressures (or low ρ_l/ρ_v). Like ρ_l/ρ_v, surface tension is an important property at all length scales; in microchannels it is especially important in dictating the well documented rapid bubble growth instability, which is strongly dependent on the bubble diameter-to-channel hydraulic diameter ratio. Since the surface tension and especially the density ratio of typical coolants like HFE-7100 are significantly lower than that of water, at least under conditions pertinent to electronic cooling, it can be hypothesized that flow instabilities are of less concern when using coolants in microchannels. However, this has yet to be shown.

* Corresponding authors. Tel.: +1 518 276 2886 (Y. Peles), +1 480 554 0593 (R. Prasher).
E-mail addresses: pelesy@rpi.edu (Y. Peles), ravi.s.prasher@intel.com (R. Prasher).

0017-9310/$ - see front matter © 2009 Elsevier Ltd. All rights reserved.
doi:10.1016/j.ijheatmasstransfer.2009.09.008

Nomenclatures

A	cross-sectional area of one channel (m^2)
D_h	hydraulic diameter (m)
G	mass flux (kg/m^2 s)
H	channel height (m)
L	channel length (m)
MC	microchannel
Nu	Nusselt number
P	pressure (kPa)
Po	Poiseuille number
p	perimeter (m)
q	heating power (W)
h	specific enthalpy (kJ/kg)
Re	Reynolds number
S	surface area of one channel (m^2)
SP	single-phase
T	temperature (K)
T_{in}	inlet temperature (K)
T_{out}	outlet temperature (K)
T_{sat}	saturation temperature (K)
W	channel width (m)
c_p	specific heat (isobaric) (J/kg K)
$\dot{m}$	mass flow rate (kg/s)
q''	heat flux (W/m^2)
x	vapor quality
z	location (m)

Greek letters

μ	viscosity (Pa s)
ρ	mass density (kg/m^3)
α	void fraction
ϕ	two-phase multiplier
θ	inclination angle

Subscripts

a	acceleration
f	friction
l	liquid phase
lo	liquid only
v	vapor phase
s	system
in	inlet
out	outlet
sub	subcool
sp	single-phase
tp	two-phase

This paper reports on an experimental and numerical study of Ledinegg instability in horizontal microchannels under conditions and fluids pertinent to electronics cooling. Two fluids, water at sub-atmospheric pressures (for low saturation temperatures) and the refrigerant HFE-7100, were used with a range of heat fluxes, mass fluxes, and channel hydraulic diameters. Flow conditions corresponded to single-phase, stable two-phase, and unstable two-phase flow. The onset of flow instability (OFI) was determined, and the slope of the pressure drop–mass flux curve was closely examined to quantify the susceptibility of the system to the Ledinegg instability. Based on the demand curve slope derived from the momentum equation, systematic parametric studies are given to measure the instability's susceptibility. Increased system pressure stabilized the flow, and it was hypothesized that this had a significant effect on the improved stability of HFE-7100 compared to water. Several studies [1,15] implicitly suggest that increasing the number of parallel channels destabilized the flow. The effect of heat flux, inlet temperature subcooling, and channel hydraulic diameter were less conclusive, and they can destabilize or stabilize the flow.

2. Background

As discussed by Bouré et al. [15] and Appendix A, flow boiling in a channel is susceptible to static Ledinegg instability when the slope of the demand pressure drop–mass flux curve becomes algebraically smaller than the loop supply pressure drop–mass flux curve:

$$\left.\frac{\partial(\Delta P)}{\partial G}\right|_{channel\ demand} \leqslant \left.\frac{\partial(\Delta P)}{\partial G}\right|_{pump\ supply} \quad (1)$$

To better understand this instability, consider the channel pressure drop demand curve as a function of mass flux for constant heat flux (Fig. 1). When the flow rate is large, the flow is liquid single-phase (the right region of the curve). As the mass flux is continuously reduced while other conditions are unchanged, boiling will commence at some pressure drop (designated as onset of nucleate boiling (ONB) on the curve). Further reduction in the mass flux will gradually cause vigorous boiling. Since frictional and accelerational pressure drops tend to increase as the void fraction (and mass quality) increases, a point can be reached in which the $\Delta P - G$ slope reaches a minimum. This point is frequently termed the onset of flow instability (OFI) (see, for instance, Kennedy et al. [16]). It should be noted that the use of the term "instability" might be misleading since it does not necessarily mean that the system will become unstable beyond this point. It merely suggests that beyond this point any reduction in the mass flux can cause the flow to become unstable if proper measures are not taken.

To maintain system stability, the pump supply curve needs to be considered. If the slope of the pump supply curve (Curve A)

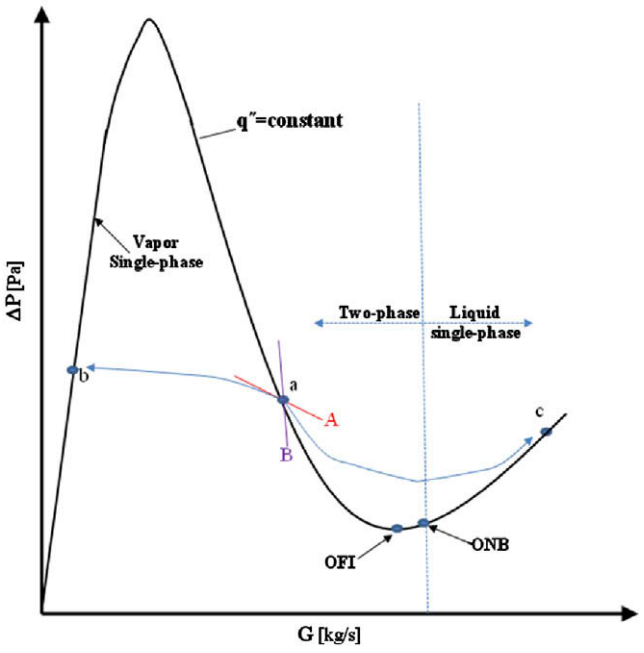

Fig. 1. Channel demand curve: pressure drop vs. mass flux for constant heat flux (qualitative representation of Fig. 2 from Boure et al. [15]).

has a smaller negative value compared to that of the demand curve, the system is unstable. This situation occurs because the pump cannot counteract even a small perturbation in mass flux from the equilibrium condition (Point *a*), and a spontaneous shift to a more stable flow condition will occur (e.g., from Point *a* to Point *b* or Point *c* in Fig. 1). Such circumstances also can occur when the supply curve has a constant pressure characteristic, i.e., when the flow is supplied between two constant pressure reservoirs. On the other hand, if the pump supply curve (Curve *B*) has a greater negative slope than that of the demand curve, the system is stable. This can be achieved, for instance, by installing a constant displacement pump, which has an almost infinite slope (i.e., *G* is fixed regardless of the pressure drop). For this reason most studies performed on flow boiling typically use a constant displacement pump instead of constant pressure drop reservoirs for forcing the flow through the channel [1,15].

Maintaining the stability of the flow can also be achieved by installing a throttling valve at the inlet of the channel, which can moderate the negative slope of the demand curve if the added pressure drop across the inlet restrictor is high enough, as shown in Fig. 2. If the pressure drop curve of a throttling valve (Curve *A*) is added to the demand curve of the channel (Curve *B*), the total system pressure drop (i.e., the throttling valve together with the channel) versus mass flux of the modified system is constructed (Curve *C*). As can be seen, for example, at Point *a*, the slope of the unmodified channel is negative and is susceptible to the Ledinegg instability. However, with the modified channel, the slope of the curve at Point *b* is positive and, hence, the Ledinegg instability is not possible. Thus, the system with the throttling valve is much more resistant to the Ledinegg instability. Note that for this to happen the pressure drop of the throttling valve must be sufficiently large so that the slope of the modified system can become positive. One obvious consequence of utilizing a throttling valve is the increased pressure drop required to deliver the flow through the system.

It should be noted that the Ledinegg instability represents the limiting condition for a large bank of parallel tubes between common headers, since any individual tube sees an essentially constant pressure drop [15]. It follows that even if a constant displacement pump is used, the effective supply curve of an individual channel gradually loses its ability to withstand a Ledinegg instability with an increasing number of parallel channels.

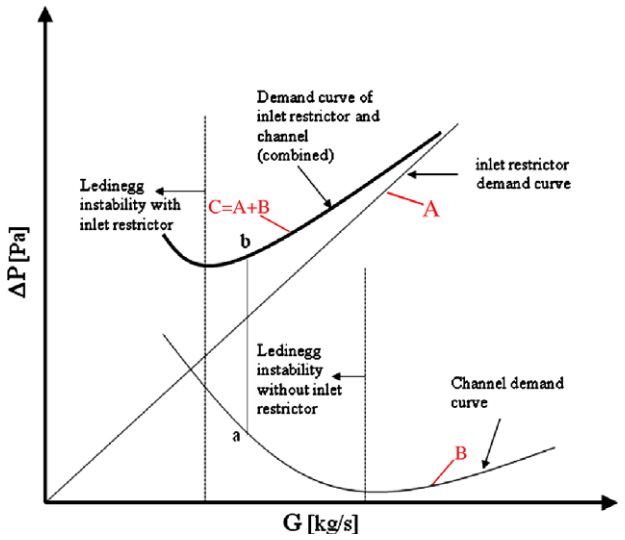

Fig. 2. The effect of installing inlet restrictor at the channel inlet. The OFI point is shifted to the left with inlet restrictor.

3. Experimental studies

3.1. Experimental apparatus and procedures

The microchannel cold plate and the test assembly are schematically depicted in Fig. 3. As shown in Fig. 3(a) and (b), the microchannel cold plate with a metallic heater fabricated on the bottom was attached on the package substrate. The substrate was mounted onto a circuit motherboard though a pin-grid-array (PGA) socket. Details on the fabrication and assembly processes of microchannel cold plate can be found in a paper by Prasher et al. [17]. Three different designs of horizontal microchannel cold plates (Units I, II, and III) were tested in the current study. The channel widths are 61, 165, and 330 μm, respectively, and the channel length/diameter ratios are 150, 68, and 45. Dimensions of microchannel cold plate are shown in Table 1, which are based on SEM measurements. Fig. 3(c) shows the SEM picture of Unit I.

The experimental setup was constructed to measure flow rate, pressure drop, and heat transfer characteristics of the microchannel cold plate. Fig. 4 shows the schematic of the experimental setup. The working fluid was continuously drawn from a stainless steel reservoir (fluid tank) by a positive displacement pump. The loop has two branches, the bypass branch and the main branch, controlled by two valves. A flow meter and a filter were plumbed in series with the microchannel cold plate in the main branch. Both branches in the loop drained to a reservoir from which the pump drew the working fluid.

A differential pressure transducer was connected to the inlet/outlet plumbing adaptors on the microchannel cold plate to measure the pressure drop across it. An absolute pressure transducer was also connected to the outlet to monitor the system pressure during experiments. A vacuum pump was connected to the reservoir for controlling the system pressure and degassing the loop. Fluid temperature in the reservoir was controlled by an external temperature controller plumbed to a heat exchanger in the reservoir. The fluid temperature was monitored by a K-type thermocouple immersed in the liquid. Thermocouples were also attached to the inlet/outlet plumbing holes of the microchannel cold plate to measure the fluid temperatures. Thermocouple readings and the voltage outputs from the flow meter and pressure transducers were taken with a data acquisition system.

Two different working fluids were tested in the current study, deionized (DI) water at a saturation pressure of 70 °C and HFE-7100 at ambient pressure condition. HFE-7100 is a highly-wetting refrigerant (methoxy-nonafluorobutane, $C_4F_9OCH_3$) [18]. Thermophysical properties of water and HFE-7100 are compared in Table 2.

A thorough degassing was carried out before starting each test. For water, the system pressure was first reduced to a preset level by running the vacuum pump, while for HFE-7100, the system pressure was maintained at atmospheric pressure. After the preset level of system pressure was reached, the vacuum valve was closed. The external temperature controller was then turned on to heat the fluid inside the reservoir (fluid tank) slightly higher than the saturation point to make sure the fluid boiled, and at the same time, the system pump continuously circulated the fluid in the loop. The vacuum line valve was opened periodically to evacuate the purged non-condensable gasses in the reservoir and to relieve the system pressure back to the preset level. This degassing procedure was conducted for more than 2 h before experiments begun. Uncertainties of measured values are given in Table 3.

3.2. Experimental observations

Fig. 5 shows that for water the experimental pressure drop is approximately V-shaped with respect to the mass flux. It can be seen that in the single-phase regime (higher flow rate portion)

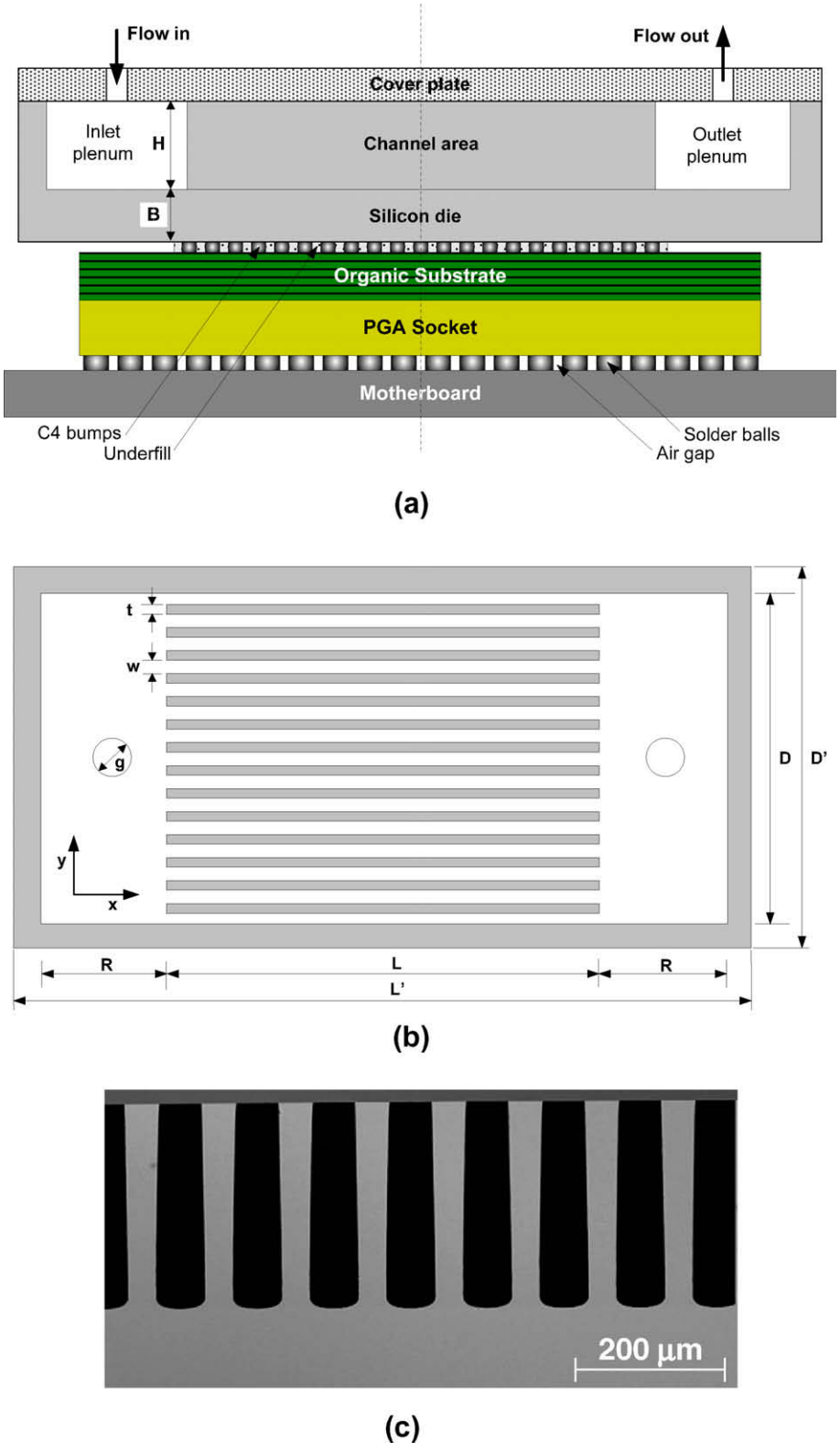

Fig. 3. (a) Cross-sectional view of the microchannel cold plate assembly. (b) Top view of microchannel cold plate. (c) SEM cross-section of the microchannel array of Unit I.

pressure drop is proportional to flow rate on the whole. As the flow rate reduces the pressure drop decreases until a point when the flow makes a transition to two-phase state and starts to increase. Beyond the boiling incipience point, liquid in contact with the channel walls gets superheated above the local saturation point leading to phase change. Similar trends were observed by earlier researchers like in Refs. [1,15]. The vaporized fluid leads to a rapid increase of the pressure drop over that of single-phase flow, mainly attributed to the accelerational (due to difference in the mass density of the liquid and vapor) and additional frictional losses of the vapor/liquid mixture flow [15]. Experimental data in Fig. 5 also show that in the single-phase region the pressure drop is lower

Table 1
Dimensions of the microchannel cold plates.

Parameters	Unit I	Unit II	Unit III
Number of channels	100	40	25
Channel width (W, μm)	61	165	340
Channel height (H, μm)	272	330	335
Channel length (L, mm)	15	15	15
Hydraulic diameter (D_h, μm)	100	220	337
Fin thickness (t, μm)	39	90	80
Eff. cross-sectional area (A_{cross}, mm^2)	1.66	2.18	2.85
MC region width (D, mm)	10	10	10
MC region length (L, mm)	15	15	15
Plenum size (mm^2)	4 × 10	4 × 10	4 × 10
Inlet/outlet hole size (g, mm)	1	1	1
Inlet/outlet plenum size (R, mm)	4	4	4
Cold plate width (D', mm)	16	16	16
Cold plate length (L', mm)	27	27	27

Table 2
Thermo-physical properties of HFE-7100 and water.

Properties	HFE-7100	Water
Boiling point (1 atm), °C	61	100
Critical temperature, °C	195.3	374
Critical pressure, MPa	2.23	22.06
Heat capacity, kJ/kg K	1.17	4.18
Latent heat at saturation (1 atm), kJ/kg	111.6	2261
Density (at 45 °C), kg/m^3	1450	990
Thermal conductivity (liq. at 40 °C), W/m K	0.06	0.6
Viscosity (liq. at 40 °C), μPa s	~450	~650
Surface tension, N/m (70 °C)	0.0136	0.065

Table 3
Uncertainties of different variables.

Measurement	Uncertainties
Flow rate	±0.25 ml/min
Absolute pressure transducer	±500 Pa
Differential pressure transducer	±180 Pa

for higher power. This is due to increase in the average liquid temperature which in turn reduces the viscosity of the liquid. In the two-phase region, higher heat power vaporizes more liquid, thus the overall fluid flow is of higher void fraction, resulting in greater density change and larger frictional pressure loss through microchannels. Therefore, the overall pressure drop increases with the heat inputs, as observed in each subplot of Fig. 5.

Although the general trend is same, the total pressure drop keeps increasing as the flow rate reduces in two-phase flow regime and it increases with the flow rate in subcooled liquid regime, different pressure-drop slopes can be observed by comparing Fig. 5(a)–(c). For the smaller channels of Unit I, the pressure drop-mass flux characteristic curve in two-phase region is much steeper, which suggests that Unit I should be more susceptible to flow instability at mass fluxes smaller than at OFI. However, the mass flux at OFI for Unit I is lower than for Unit III (Fig. 5), which is in agreement with earlier study for water in macrochannels [28] that suggests that the mass flow at OFI for fixed power input would increase when the ratio L/D_h decreases. In addition, the experimental flow temperature measurements from the horizontal microchannel heat sink (Unit I) are included in Fig. 6 to provide enough information for subsequent modeling and analysis. The error bound after OFI point (negative slope region) in Figs. 5 and 6 represents the self-sustained periodic fluctuations in the pressure drop and temperature with respect to time. This is mainly caused by dynamic two-phase flow instability (well-known pressure-drop flow oscillations). All the above experiments are limited to the common fluid – water. When the coolant HFE-7100 is used as the working fluid in microchannels, the pressure drop–flow rate characteristic curve even in Unit I becomes much more flat, as depicted in Fig. 7, during single-phase and flow boiling regimes. By comparing the experimental results in Figs. 5(a) and 7, it is observed that the HFE-7100 can transition to annular boiling flow at much higher mass flow rate under the same heat input, because in microchannels bubbly flow corresponding to nucleate boiling is more likely to occur with a low surface tension coolant, such as HFE-7100.

4. Theoretical modeling

The discussion in Section 2 and experimental results in Section 3 have shown that the pressure drop can, and often does, have a local minimum at mass fluxes lower than the onset of nucleate boiling. With the reduction of mass flow rate, following boiling incipience, the frictional and accelerational pressure drops can increase more rapidly with increasing void fraction than decrease due to decreases in the mass flux. Hence, the pressure drop increases with decreasing mass flux.

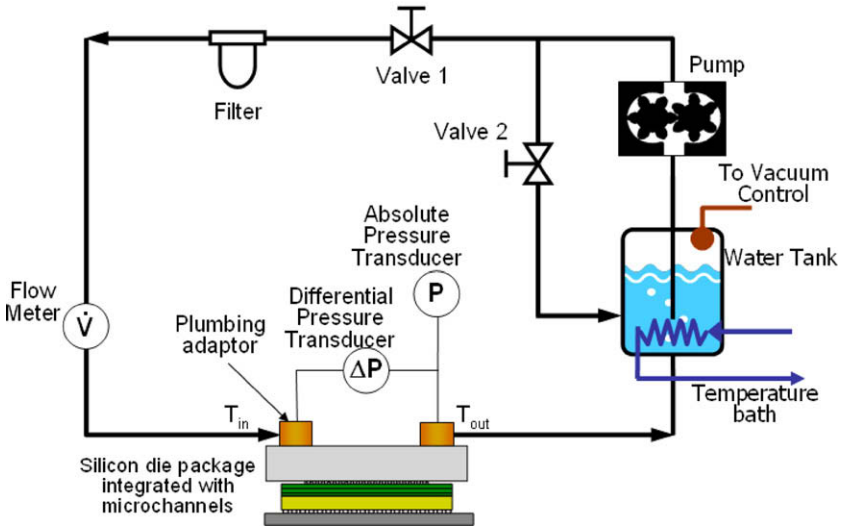

Fig. 4. Schematic of flow loop setup.

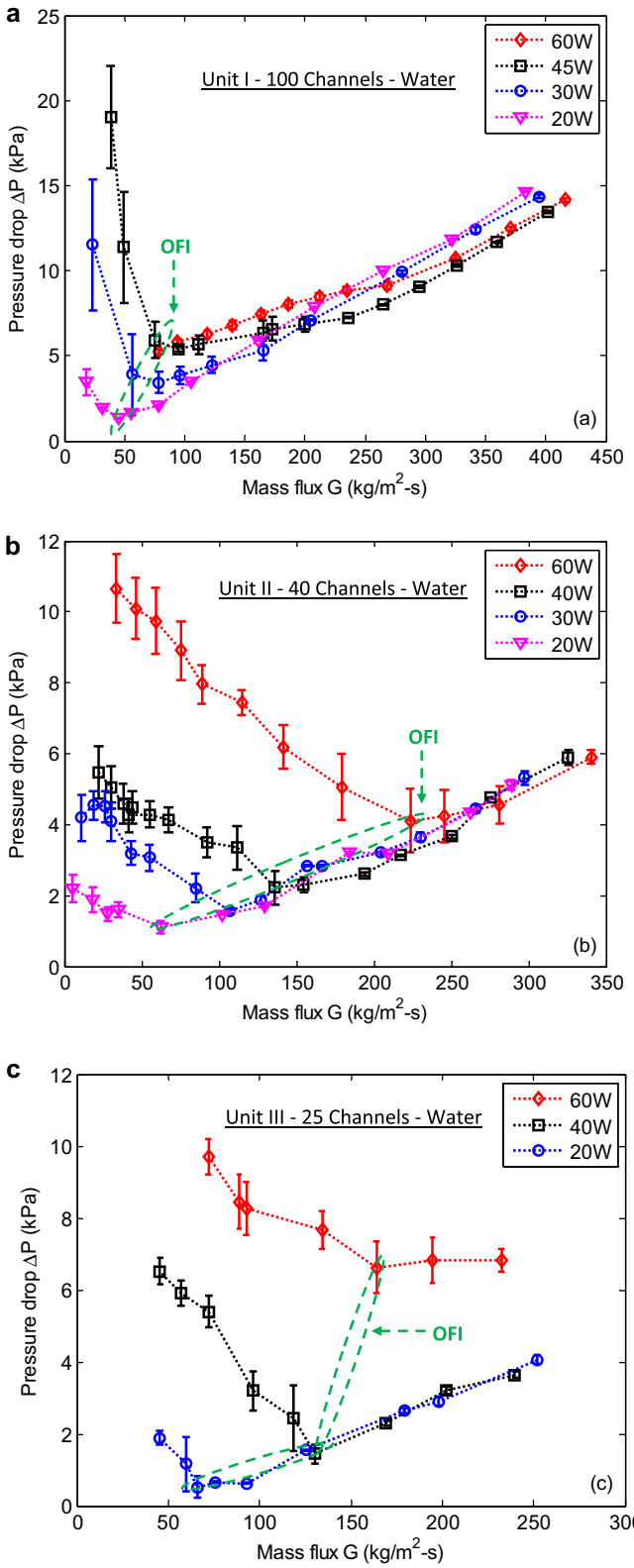

Fig. 5. Comparison of water experimental data with different number of parallel channels. (a) Unit I (100 parallel channels), (b) Unit II (40 parallel channels), and (c) Unit III (25 parallel channels) (lines used for clarity).

As mentioned earlier, the susceptibility of flow boiling systems to the Ledinegg instability can be examined through the pressure drop–mass flux demand curve at a fixed heat flux. Any discussion about this flow instability should be resolved through knowledge

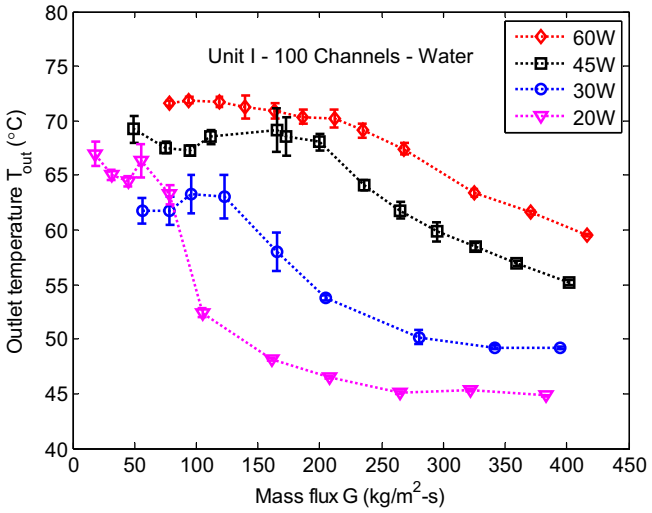

Fig. 6. Experimental outlet temperature measurements of microchannel heat sink (Unit I) at different heat inputs (error bar: temperature fluctuation).

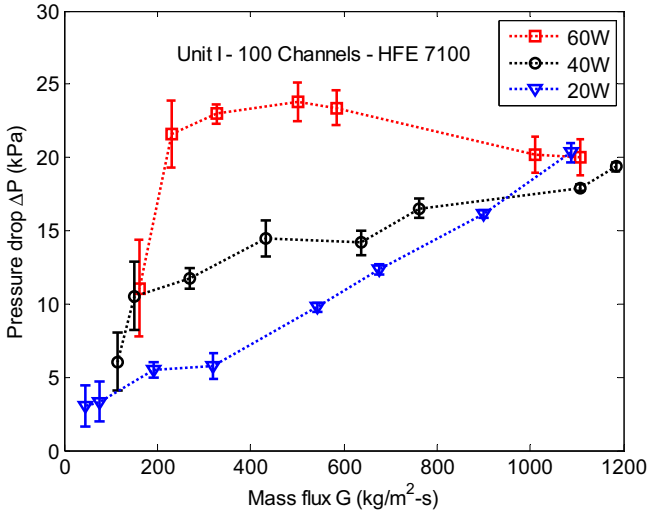

Fig. 7. Experimental pressure drop–mass flux characteristics for HFE-7100 in Unit I with 100 channels, $D_h = 100$ μm, $L = 15$ mm, at different heat inputs and reduced pressure ~0.045 (error bar: pressure drop fluctuation).

of the curve. Therefore, it is essential to model and analyze the above experimental two-phase flow characteristics for potential flow instability studies; some preliminary discussions on mass, energy and momentum conservation principles are included in Appendix A. Single-phase pressure drop model is initially discussed in Section 4.1, followed by the two-phase flow characteristics in Section 4.2, where particular interest is focused on the pressure-drop slope at lower mass fluxes.

4.1. Single-phase pressure drop

During single-phase experiments, the flow was kept laminar. The pressure drop for laminar fully-developed single-phase flow across a microchannel can be written as a function of the mass flux (kg/m^2 s), G, according to [19]

$$\frac{dP_f}{dz} = \frac{4\tau}{D_h} = \frac{2f \cdot G^2}{\rho \cdot D_h} \tag{2}$$

The friction factor is

$$f = \frac{Po}{Re_{D_h}} = \frac{Po \cdot \mu}{G \cdot D_h} \tag{3}$$

where μ the dynamic viscosity and $Re_{D_h} \equiv GD_h/\mu$ is the channel Reynolds number. Po is the Poiseuille number, which depends on the flow-channel geometry. For a rectangular channel with a short side a, a long side b, and the channel aspect ratio, $\alpha_c = a/b$, the Poiseuille number is, $Po = 24 \cdot (1 - 1.3553\alpha_c + 1.9467\alpha_c^2 - 1.7012\alpha_c^3 + 0.9564\alpha_c^4 - 0.2537\alpha_c^5)$, as given by [24]. Entrance (developing flow) effects can be included, but its impact on the total pressure drop is very small. Therefore, according to Eqs. (2) and (3), in the single-phase regime, the pressure drop is related to the size of the microchannel roughly by $\Delta P \sim D_h^{-2}$ at a given *mass flux*. Eqs. (2) and (3) suggest that in the laminar regime, the pressure drop across a microchannel is linearly proportional to the mass flow rate and kinematic viscosity (μ/ρ). Experimental data in Figs. 8 and 9 show that pressure drop in the single-phase regime is directly proportional to G and is lower for higher heat transfer rates because of reduced liquid viscosity with increased wall temperatures.

4.2. Two-phase pressure drop

Following boiling inception, the pressure drop (ΔP_{total}) in the channel can be divided into two regions: one for liquid single-phase flow that starts at the inlet, and one for flow boiling, i.e.,

$$\Delta P_{total} = \Delta P_{sp} + \Delta P_{tp} \tag{4}$$

where ΔP_{sp} is the single-phase pressure drop and ΔP_{tp} is the two-phase pressure drop. If boiling inception is assumed to occur at $x = 0$, the single-phase pressure drop can be obtained using Eq. (2) in conjunction with an energy balance. While there have been several successful attempts to develop two-phase frictional pressure drop models in microchannels, the well established semi-empirical correlation of Lockhart–Martinelli [20] has shown to hold at the micro scale [21–24], provided the correlation's C-factor (see Eq. (7)) is properly modified to account for scale effects. The pressure drop for diabatic two-phase flow is comprised of frictional, accelerational, and gravitational pressure drops and is expressed as follows [26]:

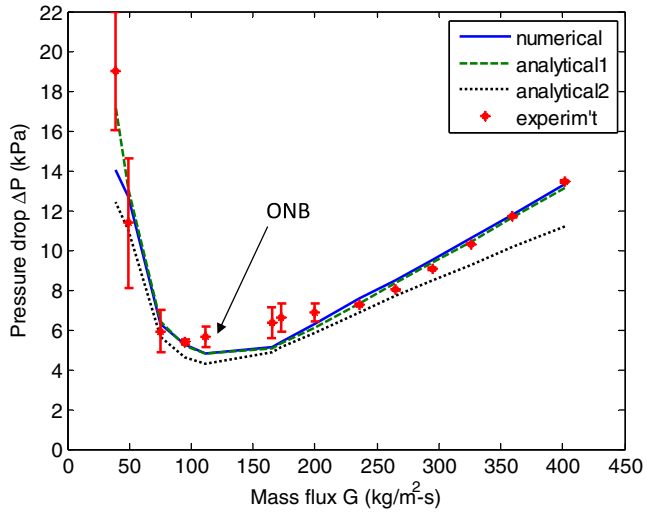

Fig. 8. Comparison of theoretical and experimental steady-state flow characteristics at the 45 W heat input (solid line: numerical model; dashed line: analytical model based on system pressure and temperature $P_s = \frac{P_{in}+P_{out}}{2}, T_s = \frac{T_{in}+T_{out}}{2}$; dotted line: analytical model based on system pressure and temperature $P_s = P_{in}$, $T_s = \frac{T_{in}+T_{sat}(P_{in})}{2}$; $*$: experiment; error bar: pressure drop fluctuation) for water.

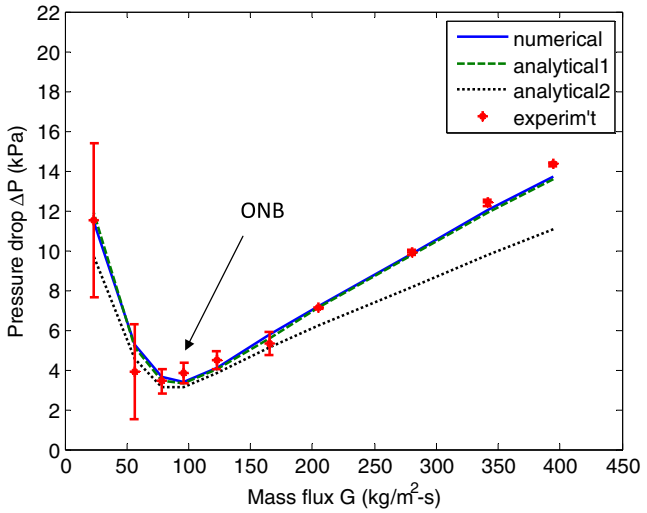

Fig. 9. Comparison of theoretical and experimental steady-state flow characteristics at the 30 W heat input (solid line: numerical model; dashed line: analytical model based on system pressure and temperature $P_s = \frac{P_{in}+P_{out}}{2}, T_s = \frac{T_{in}+T_{out}}{2}$; dotted line: analytical model based on system pressure and temperature $P_s = P_{in}$, $T_s = \frac{T_{in}+T_{sat}(P_{in})}{2}$; $*$: experiment; error bar: pressure drop fluctuation) for water.

$$(\Delta P)_{tp} = \underbrace{\frac{2f_{lo}G^2L_{tp}}{\rho_l D}\left[\frac{1}{x_0}\int_0^{x_0}\phi_{lo}^2\,dx\right]}_{\text{frictional pressure drop}} + \underbrace{\frac{G^2}{\rho_l}\left[\frac{x_0\rho_l}{\alpha_0\rho_v} + \frac{(1-x_0)^2}{(1-\alpha_0)} - 1\right]}_{\text{accelerational pressure drop}} + \underbrace{\frac{gL_{tp}\sin\theta}{x_0}\int_0^{x_0}[\rho_v\alpha + \rho_l(1-\alpha)]dx}_{\text{gravitational pressure drop}} \tag{5}$$

where the last gravitational term is neglected in this paper for horizontal channels, L_{tp} is the length of two-phase flow region, f_{lo} is the friction factor, and v_l and v_v are the specific liquid and gas volumes, respectively. x_0 and α_0 are the exit quality and void fraction, respectively. ϕ_{lo}^2 is the two-phase frictional multiplier defined as

$$\phi_{lo}^2 = \frac{(dP/dz|_f)_{tp}}{(dP/dz|_f)_{lo}} \tag{6}$$

$(dP/dz|_f)_{tp}$ is the frictional pressure drop gradient of the two-phase mixture and $(dP/dz|_f)_{lo}$ is the single-phase pressure gradient assuming the total flow (liquid plus vapor) considered as liquid. The Lockhart–Martinelli correlation also uses a slightly different two-phase multiplier defined as

$$\phi_l^2 = \frac{(dP/dz|_f)_{tp}}{(dP/dz|_f)_l} = 1 + \frac{C(1-e^{-319D_h})}{X} + \frac{1}{X^2} \tag{7}$$

where

$$\phi_{lo}^2 = \phi_l^2(1-x)^2\frac{f_l}{f_{lo}}, \quad X = \frac{(dP/dz|_f)_l}{(dP/dz|_f)_v} \tag{8}$$

Here $(dP/dz|_f)_l$ and $(dP/dz|_f)_v$ are the single-phase pressure gradients assuming the liquid phase and gas phase to flow alone in the channel, respectively. f_l is the friction factor for the liquid flowing alone in the channel. The constant C is an empirically defined factor, which depends on the flow regime (laminar, turbulent, or a combination of the two) and flow morphology (e.g., bubbly, intermittent, etc.) among other parameters. Conventional scale studies suggest that for liquid laminar and vapor laminar flows, the value of the constant C is 5 [21–24], which is used in this microchannel fluid flow study. Based on previous minichannels and microchannels results [21–23], Kandlikar [24] suggested to modify the C-factor of the

two-phase multiplier, ϕ_l^2, in diminishing length scales according to Eq. (7). And the void fraction for annular flow is given by the following correlation [25]:

$$\alpha = 1 - \frac{1}{\sqrt{\phi_l^2}} \tag{9}$$

Integrating with respect to quality the two-phase multiplier, ϕ_{lo}^2, in Eq. (5), yields the explicit pressure drop function:

$$\begin{aligned}\Delta P = {} & \frac{2Po\cdot\mu_l\cdot G\cdot(L-z_s)}{\rho_l\cdot D_h^2\cdot x_0}\left(x_0-\frac{x_0^2}{2}+\frac{x_0^2}{2c}+\frac{5-5\exp(-319D_h)}{8\sqrt{c}}\right.\\ & \times\left[\arcsin(2x_0-1)+\frac{\pi}{2}\right]+\frac{5-5\exp(-319D_h)}{16\sqrt{c}}\\ & \left.\times\sin[2\arcsin(2x_0-1)]\right)+\frac{2Po\cdot\mu_l\cdot\boldsymbol{G}\cdot z_s}{\rho_l\cdot D_h^2}\\ & +\frac{G^2}{\rho_l}\left[\frac{x_0^2}{\alpha_0}\frac{\rho_l}{\rho_v}+\frac{(1-x_0)^2}{1-\alpha_0}-1\right]\end{aligned} \tag{10}$$

where $c=\frac{\mu_l}{\mu_v}\frac{\rho_v}{\rho_l}$, $X^2=c\left(\frac{1-x_0}{x_0}\right)$, $\alpha_0=1-\left(1+\frac{5-5\exp(-319D_h)}{X}+\frac{1}{X^2}\right)^{-1/2}$, and z_s is the location for boiling incipience. The right hand side is the summation of the two-phase frictional pressure drop (first term), the single-phase frictional pressure drop (second term), and the accelerational pressure drop (third term).

Taking the derivative of the pressure drop with respect to the mass flux, G, yields the following expression:

$$\begin{aligned}\frac{\partial(\Delta P)}{\partial G} = {} & \frac{2Po\cdot\mu_l\cdot(L-z_s)}{\rho_l\cdot D_h^2\cdot x_0}\left(x_0-\frac{x_0^2}{2}+\frac{x_0^2}{2c}+\frac{5-5\exp(-319D_h)}{8\sqrt{c}}\right.\\ & \times\left[\arcsin(2x_0-1)+\frac{\pi}{2}\right]+\frac{5-5\exp(-319D_h)}{16\sqrt{c}}\\ & \left.\times\sin[2\arcsin(2x_0-1)]\right)+\frac{2Po\cdot\mu_l\cdot z_s}{\rho_l\cdot D_h^2}\\ & +\frac{2G}{\rho_l}\left[\frac{x_0^2}{\alpha_0}\frac{\rho_l}{\rho_v}+\frac{(1-x_0)^2}{1-\alpha_0}-1\right]\end{aligned} \tag{11}$$

Since the pressure drop gradient $\partial(\Delta P)/\partial G$ can be explicitly calculated, the analytical model can be used to evaluate flow stability. However, the analytical model assumes a constant system pressure [26], while the pressure drop during the experiments varied by up to 50% of the system exit pressure as calculated from the numerical model (see discussion below) and shown in Figs. 10a and 10b. To elucidate this large system pressure excursion on the model prediction, two different pressure/temperature methods were used to calculate the fluid properties in Eqs. (10) and (11):

$$\text{Case 1}:\ P_s=\frac{P_{in}+P_{out}}{2},\ T_s=\frac{T_{in}+T_{out}}{2},\ \rho_l=\rho(P_s,T_s),\ \mu_l=\mu(P_s,T_s)$$

$$\text{Case 2}:\ P_s=P_{in},\ T_s=\frac{T_{in}+T_{sat}(P_{in})}{2},\ \rho_l=\rho(P_s,T_s),\ \mu_l=\mu(P_s,T_s)$$

where T_{in} and T_{out} are the experimental temperature measurements at the channel inlet and exit, respectively. In Case 1, both inlet/exit experimental conditions were used to obtain the pressure and temperature, while in Case 2 only the inlet pressure was used. For Case 2, this resulted in large deviations between the analytical and experimental data as shown in Figs. 8 and 9, while Case 1 showed good agreement between the experimental data and the numerical prediction. However, it is not practical to use both inlet and outlet operating conditions for model prediction, and more generally, only one-side pressure and temperature data are used to predict the other, as used in Case 2. As seen from Figs. 8 and 9, the predictions for Case 2 are with larger modeling error even in single-phase region, which is caused by the relative large pressure change along the microchannel. Therefore, because of the significant pressure drop, fluid properties like density and viscosity also change greatly in microchannels. It follows that fixed mean fluid properties are no longer good assumptions in analytical model calculations (10) and (11) for microchannels, a big difference between conventional and micro scale two-phase flow modeling methods is expected.

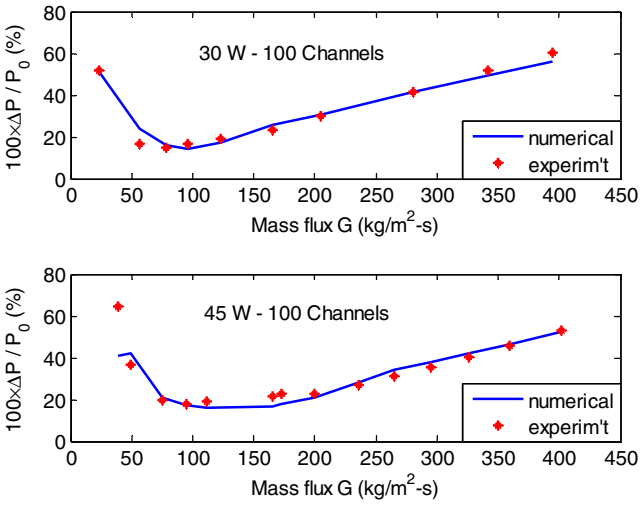

Fig. 10a. Experimental and calculated relative pressure ratios at 30 and 45 W for water.

For improved accuracy, it is desirable to account for the changes of the system pressure in the pressure drop model. Unfortunately, with a variable system pressure, the derivative of the explicit pressure drop function is not readily obtained due to fluid property changes along the length. Therefore, a numerical method was developed, and, for simplicity, a one-dimensional pressure gradient model was used. Since constant heat flux boundary conditions are considered here, the enthalpy distribution along the channel is linear as discussed in Appendix A and Eq. (27); that is, for any location ($z \in [0, L]$)

$$h_z = h_{in} + \frac{q''\cdot S\cdot z}{G\cdot A\cdot L} \tag{12}$$

where S is the surface area and A is the cross-sectional area.

Thus, the pressure gradient for the two-phase flow [1,25,26] can be calculated by

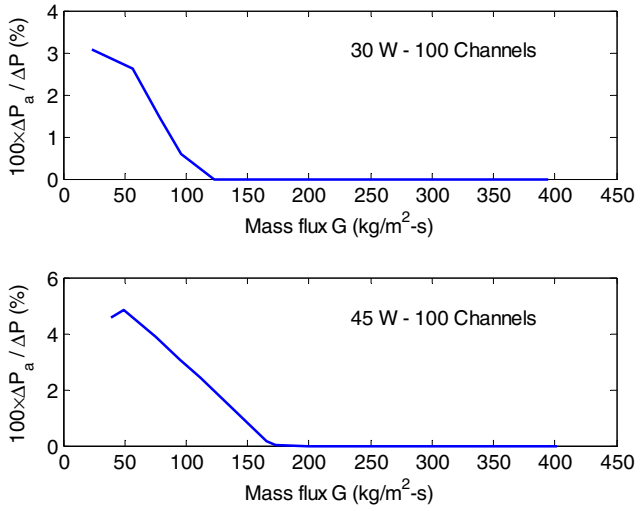

Fig. 10b. Calculated accelerational pressure drop contribution at 30 and 45 W for water.

$$\left(\frac{dP}{dz}\right)_{tp} = \left(\frac{dP_f}{dz}\right)_l \phi_l^2 + \frac{d}{dz}\left(\frac{G^2(1-x)^2}{\rho_l(1-\alpha)} + \frac{G^2x^2}{\rho_v\alpha}\right) + [\rho_v\alpha + \rho_l(1-\alpha)]g\sin\theta \tag{13}$$

where the terms on the right hand side accounts for friction, acceleration, and gravitation (absent for horizontal channels), respectively. The momentum equation (13) is a simplified form of the well-known drift-flux model in steady state [1]. The two-phase multiplier ϕ_l^2 is given in Eq. (7), and α given in Eq. (9). The gradient of Eq. (13) is a spatial ordinary differential equation and can be solved numerically by using a commercial toolbox such as Matlab®. The numerical model also provided detailed predictions of the pressure distribution in the channel as shown in Fig. 11, where different boiling conditions correspond to different mass fluxes but similar heat fluxes.

Although the above numerical model (13) can predict the spatial pressure distribution along the channel, the pressure drop–mass flow rate slope under different operating conditions is the main concern for two-phase flow instability studies. For a given working fluid, the flow characteristics usually depends on system pressure, mass flux, inlet subcooling, heat flux, and channel size. When studying the individual effects, one may fix other attributes; then imposing reasonable positive and negative perturbations on mass flux G, those are, G^+ and G^-, based on the numerical model (13), one can calculate the corresponding pressure drop, ΔP^+ and ΔP^-. Thus, the numerical pressure drop–mass flux slope can be obtained by

$$\frac{\partial(\Delta P)}{\partial G} = \frac{\Delta P^+ - \Delta P^-}{G^+ - G^-} \tag{14}$$

which will be used in the subsequent parametric instability studies.

To validate the numerical model, the model results were compared to the experimental data at similar conditions. The agreement between the experiments and the modeling results was assessed using a mean absolute error (MAE):

$$MAE = \frac{1}{M}\sum \frac{|\Delta P_{mod} - \Delta P_{exp}|}{\Delta P_{exp}} \times 100\% \tag{15}$$

As shown in Figs. 8 and 9, for single-phase flow both models follow very closely the experimental results. During water flow boiling, the measured pressure drop fluctuations were relatively large due to periodic dynamic flow instabilities. Within these fluctuations the numerical model successfully predicted the mean experimental results (Fig. 10a) as evidenced by the small MAE at heat flux of 45 W (MAE = 9.0%) and at 30 W (MAE = 7.8%), while the MAE for the analytical model (10) in Case 2 is about 15%. As discussed earlier, the two-phase pressure drop, ΔP_{tp}, consists of the frictional pressure drop, ΔP_f, and the accelerational pressure drop, ΔP_a. As shown in Fig. 10b, the accelerational pressure drop is only a small fraction of the total pressure drop (less than 3%) and, thus, was neglected.

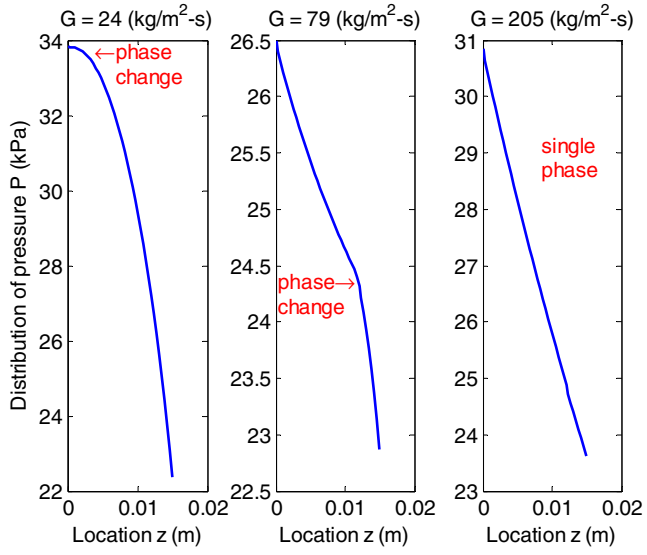

Fig. 11. Pressure distribution for different steady-state mass fluxes at the 30 W heat input for water.

5. Results and discussion

As discussed earlier, the susceptibility of flow boiling systems to the Ledinegg instability can be examined through the pressure drop–mass flux demand curve at a fixed heat flux. Therefore, two-phase pressure drop characteristics are initially discussed in this section, with particular interest on the gradient of the slope at lower mass fluxes, which is presented in Section 5.1. Since a throttling valve can alleviate instabilities, we also quantitatively examine its effect on the pressure drop demand curve and provide some guidelines to properly size a valve to mitigate instabilities. Section 5.2 is, therefore, devoted to the discussion of throttling valves and their effects on system stability.

5.1. Susceptibility to the Ledinegg instability

The susceptibility of the system to the Ledinegg instability can be assessed by considering the negative segment of the pressure drop–mass flux gradient. As the pressure drop–mass flux slope becomes steeper, the system is more likely to exhibit flow instability and, possibly, a premature critical heat flux condition can occur. It is important to acknowledge that the local minima of the pressure drop–mass flux curve does not necessarily correspond to a transition to unstable flow. This will occur only if the supply curve has a zero slope (i.e., constant pressure drop). As explained in the Background Section, for a system with a constant displacement pump (i.e., constant total mass flow rate) and finite number of parallel channels, the slope is neither zero nor infinite. There are several factors that affect the curve's slope, including heat flux, system pressure, mass quality, and channel hydraulic diameter. This can be expressed as follows:

$$\frac{d(\Delta P)}{dG} = func(P_{sat}, G, \Delta T_{sub,i}, q'', D_h, L, \text{type of fluid}) \tag{16}$$

The significance of each effect listed above is discussed below.

5.1.1. Effect of type of fluid

Fig. 7 shows the experimental pressure drop–mass flux curve for HFE-7100. When comparing this figure and Figs. 8 and 9, it is evident that the shape of the HFE-7100 curve is notably different from that of water. There are two primary causes for these differences, namely different flow patterns and different reduced pressures (P/P_c) at which experiments were conducted. Flow patterns affect the void fraction and the slip velocity, which, in turn, affect the pressure drop characteristics. Experimental studies have shown that in microchannels bubbly flow corresponding to nucleate boiling is more likely to occur with a low surface tension coolant, such as HFE-7100. Conversely, flow boiling of water is much more likely to result in annular flow in which slip velocities can be significant. However, different flow patterns cannot explain the marked deviation between the trends of the two fluids, especially because at high mass quality, flow patterns of the HFE-7100 will eventually transition to annular flow. It appears that the system pressure had a marked effect on the total pressure drop–mass flux slope and, more importantly, on its gradient. In

other words, the effect of type of fluid is merely a system pressure (or density) effect. The effect of system pressure is, therefore, examined below.

5.1.2. Effect of saturation pressure

Fig. 12 depicts the pressure drop and the pressure drop gradient of water as a function of channel exit pressure obtained from the numerical modeling. Since the results were obtained while keeping the inlet subcooiling and heat flux fixed, the saturated two-phase region for all cases shown in the figure is similar (i.e., the two-phase length is similar for all cases). As the system pressure increases, the pressure drop decreases, and, more importantly for the discussion here, the slope of the demand curve, $\partial(\Delta P)/\partial G$, becomes less negative; Therefore, the system becomes less susceptible to the Ledinegg instability. From the three terms comprising the pressure drop in two-phase flow (i.e., frictional, accelerational, and gravitational pressure drops), two tend to diminish with increasing system pressure, namely accelerational and frictional. As the system pressure increases, the density of the vapor increases, and to maintain a constant mass flux, its velocity decreases. Lower velocities will mitigate increasing momentum and, as a result, will moderate acceleration. However, it should be noted that accelerational pressure drop was not significant in the present study, as shown in Figs. 10a and 10b, which suggests that the improved stability at elevated pressures arises from friction.

The increased pressure drop with decreasing mass flux at constant heat flux, as shown in Figs. 8 and 9 and schematically in Fig. 1, is primarily a result of much higher kinematic viscosity of vapor than that of liquid. For lower mass flux and fixed heat load, more vapor is generated and the two-phase region expands; thus, the overall pressure drop increases, and the pressure drop versus mass flux characteristic curve shifts to the right. The effect of system pressure on the two-phase frictional pressure drop can be assessed by examining the ratio of single-phase pressure drop of the liquid phase to that of the vapor phase. This can be done through the Martinelli parameter, X. A low Martinelli parameter is indicative of increased frictional pressure drop of vapor flow relative to liquid flow. As apparent from Eq. (7), the two-phase frictional pressure drop depends on the Martinelli parameter, such that lower X will correspond to higher two-phase pressure drop. From Eq. (2) it is evident that for laminar flow the ratio depends only on the mass quality and the ratio of the kinematic viscosities of the vapor, ν_v, and liquid, ν_l, phases. Fig. 13 shows this ratio for a mass quality of $x = 0.5$ as a function of saturated temperature, which is directly related to the saturation pressure. As the saturated temperature increases so does the saturation pressure such that higher temperatures in Fig. 13 correspond to higher system pressures. As the system pressure increases, the difference between the liquid and vapor viscosities diminishes, and the increased pressure drop with increasing mass quality is not as marked. This, in turn, tends to reduce or eliminate the negative pressure drop–mass flux slope, and, therefore, alleviates the Ledinegg instability. For many applications, such as electronics cooling, fluid temperatures below 80 °C are desired. For these temperatures the saturation liquid–vapor kinematic viscosities ratio for HFE-7100 is much lower than for water. The improved stability of the HFE-7100 compared to water is primarily attributed to the much lower viscosity ratios at the reduced pressures examined in this study for HFE-7100.

5.1.3. Effect of number of channels

As shown in Fig. 5, Units II and III have fewer parallel channels than Unit I, and the range of mass flux with negative slope for pressure drop vs. mass flux (in the regime of Ledinegg instability) is higher for channels with larger hydraulic diameter, as seen from the experimental data. For example, in the power range of

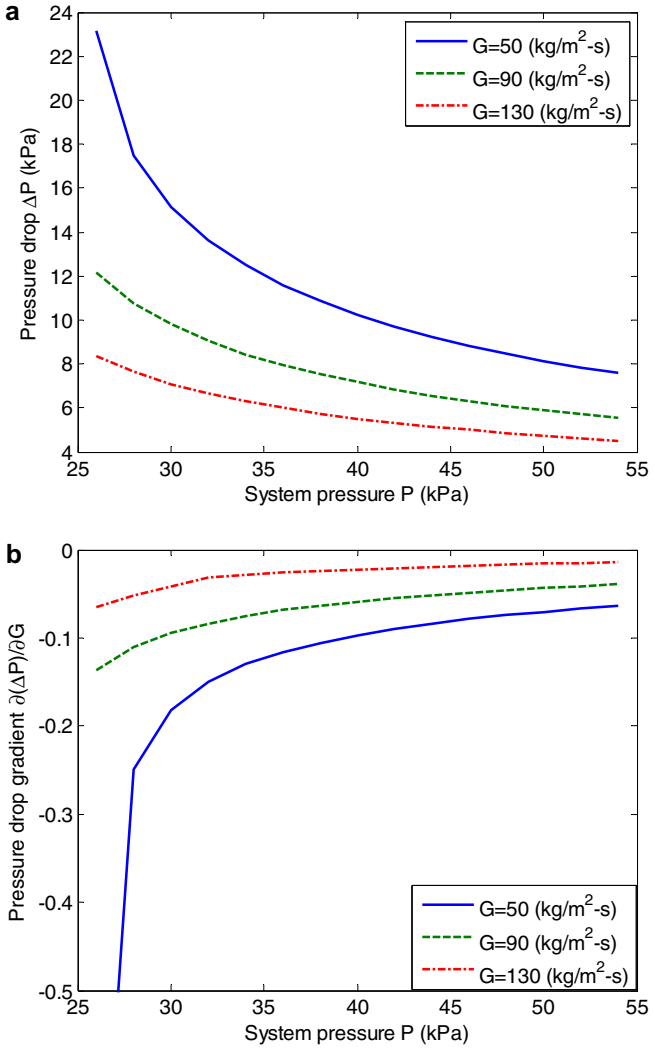

Fig. 12. The effect of pressure at fixed heat flux and inlet subcooling on (a) pressure drop and (b) pressure drop gradient under nominal conditions: $q'' \approx 44$ kW/m^2, $\Delta T_{sub} = 30$ °C, $D_h = 100$ μm, $L = 15$ mm, water.

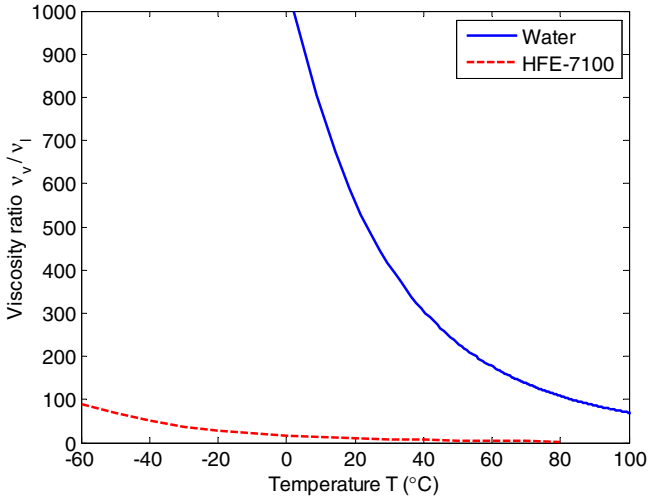

Fig. 13. Ratio between the kinematic viscosities of saturated vapor and saturated liquid for water and HFE-7100.

40–45 W, the negative slope regime for Unit I (100 channels) ranges from $G = 38.43$–75.48 kg/m^2 s, i.e., range is $\sim$37 kg/m^2 s whereas for Unit II (40 channels) and Unit III (25 channels) the range is 115 and 85 kg/m^2 s. Therefore, Units with fewer channels have a wider range of mass fluxes with more flat two-phase flow characteristics (less negative pressure drop–mass flux slope), so the system is less susceptible to the Ledinegg instability.

As discussed in the Background Section, for a system with a constant displacement pump (e.g., the present experiment) fewer parallel channels improve the stability of the flow. This can be better understood by considering two orthogonal systems: a system with a single channel, and a system with an infinite number of parallel channels. Since the pump will supply a fixed mass flow rate regardless of the pressure drop, the supply curve of the single channel system is such that $\left.\frac{\partial(\Delta P)}{\partial G}\right|_{supply} \to -\infty$, and, therefore, the following inequality is always true:

$$\left.\frac{\partial(\Delta P)}{\partial G}\right|_{demand} > \left.\frac{\partial(\Delta P)}{\partial G}\right|_{supply} \tag{17}$$

As discussed by Bouré et al. [15], such systems are unconditionally stable. When this inequality holds, the pump will be able to counteract any temporary change in the mass flow rate.

For a system with an infinite number of channels (and assuming no initial flow maldistribution) any significant mass flux change in an individual channel does not affect the total flow rate in any meaningful way. Therefore, the pressure drop between the inlet and outlet headers will not vary in response to a large change in the flow rate of an individual channel. This suggests that for the individual channel, the following relation holds: $\left.\frac{\partial(\Delta P)}{\partial G}\right|_{supply} \to 0$. Therefore, when the pressure drop–mass flux slope becomes negative the system will be unstable. For a practical system with a finite number of channels, the use of a single constant supply pump to provide the flow rate for all channels does not unconditionally mitigate the Ledinegg instability. It should be noticed that Ref. [27] presented some experimental studies on boiling flow instability between two parallel microchannels. It has been shown that the flow mal-distribution may still happen even when the positive displacement pump is used and when the stabilizing condition (17) for single channel is satisfied.

5.1.4. Heat flux effect

Fig. 14 depicts the pressure drop and $\partial(\Delta P)/\partial G$ as a function of heat flux. With all independent variables (i.e., mass flux, system pressure, inlet subcooling, channel length, hydraulic diameter, etc.) fixed, except for the heat flux, the channel segment occupied by two-phase flow increases with increasing heat flux. This is evident when considering the first law of thermodynamic for an open system in which flow boiling occupies only the channel segment corresponding to $x \geqslant 0$:

$$q''\pi D L_{SP} = G\frac{D^2}{4}c_P\Delta T_{Sub} \tag{18}$$

L_{SP} correspond to the channel length occupied by liquid single-phase flow. In Fig. 1, for a fixed mass flux, the operating conditions on the pressure drop–mass flux curve will be further to the left of the OFI for higher heat fluxes. Since the slope $\partial(\Delta P)/\partial G$ depends on the position along the pressure drop–mass flux curve it will affect the stability of the system. The slope tends to decrease fairly rapidly following onset of flow instability (in the vicinity of OFI), but this decline gradually moderates when the two-phase region occupies a considerable portion of the channel (e.g., Point *a* in the figure), and eventually the trend reverses, such that the slope begins to increase. Eventually, the pressure drop mass flux will reach a local maximum, signifying the transition to superheated vapor flow.

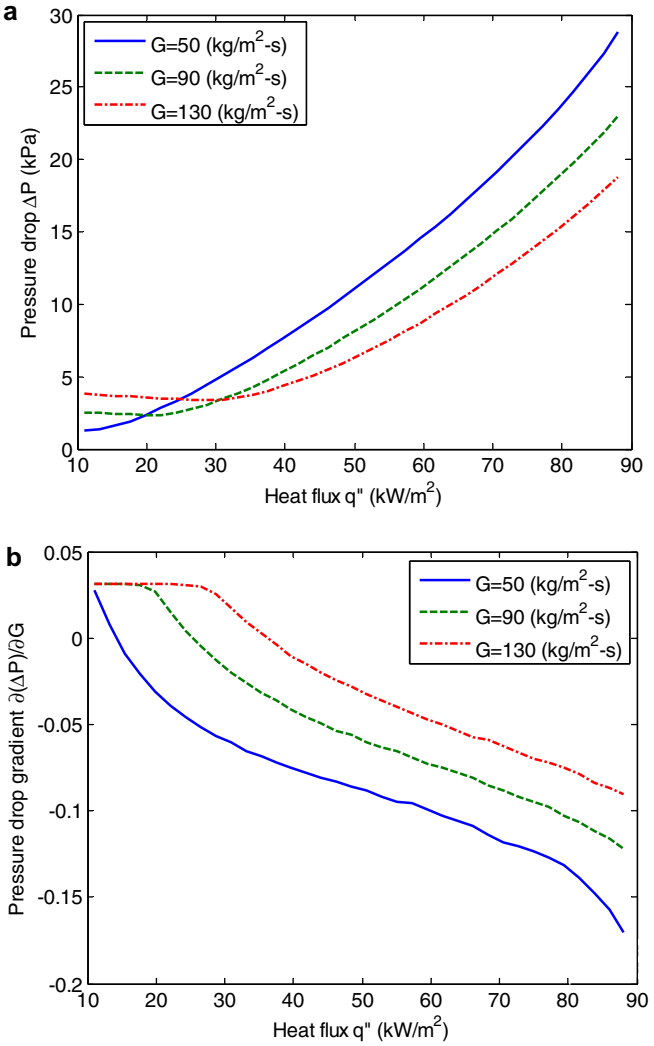

Fig. 14. The effect of heat flux at fixed pressure and inlet subcooling on (a) pressure drop and (b) pressure drop gradient under nominal conditions: $\Delta T_{sub} = 30\ ^\circ$C, $P_{in} = 45$ kPa, $D_h = 100\ \mu$m, $L = 15$ mm, water.

5.1.5. Inlet subcooling effect

Inlet subcooling and heat flux effects are interrelated; increased subcooling has an effect similar to that of decreased heat flux and vice versa. This implies that $\partial(\Delta P)/\partial G$ will have a local minimum (Fig. 15), such that the system will initially become more susceptible to the Ledinegg instability with decreased subcooling at high subcooling (for conditions near the OFI), and, eventually, become more stable at low subcooling (when the flow is primarily vapor).

5.1.6. Channel size effect

As shown in Fig. 16 and similar to the inlet subcooling, the channel hydraulic diameter is interlinked with the heat flux, such that decreased channel diameter tends to have an effect similar to that with decreased heat flux or increasing subcooling. This can be better understood when considering Eq. (18). It is evident that with decreased channel size, the two-phase region is increased. However, as implied by Eq. (8), the two-phase multiplier, ϕ_l^2, depends on the hydraulic diameter, such that the overall effect of decreasing diameter is somewhat different than decreasing the heat flux or increasing subcooling. Moreover, the effect of channel length is depicted in Fig. 17, which shows the system is more susceptible to the Ledinegg instability with the increased channel length. These trends are similar to the effect of heat flux since

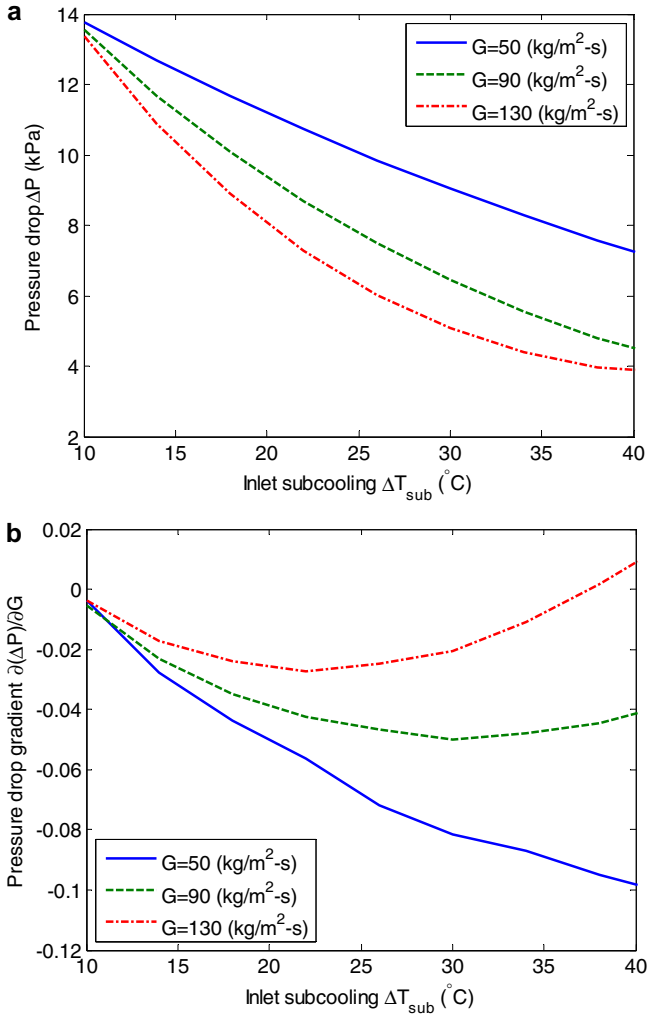

Fig. 15. The effect of inlet subcooling at fixed pressure and heat flux on (a) pressure drop and (b) pressure drop gradient under nominal conditions: $q'' \approx 44$ kW/m^2, $P_{in} = 45$ kPa, $D_h = 100$ μm, $L = 15$ mm, water.

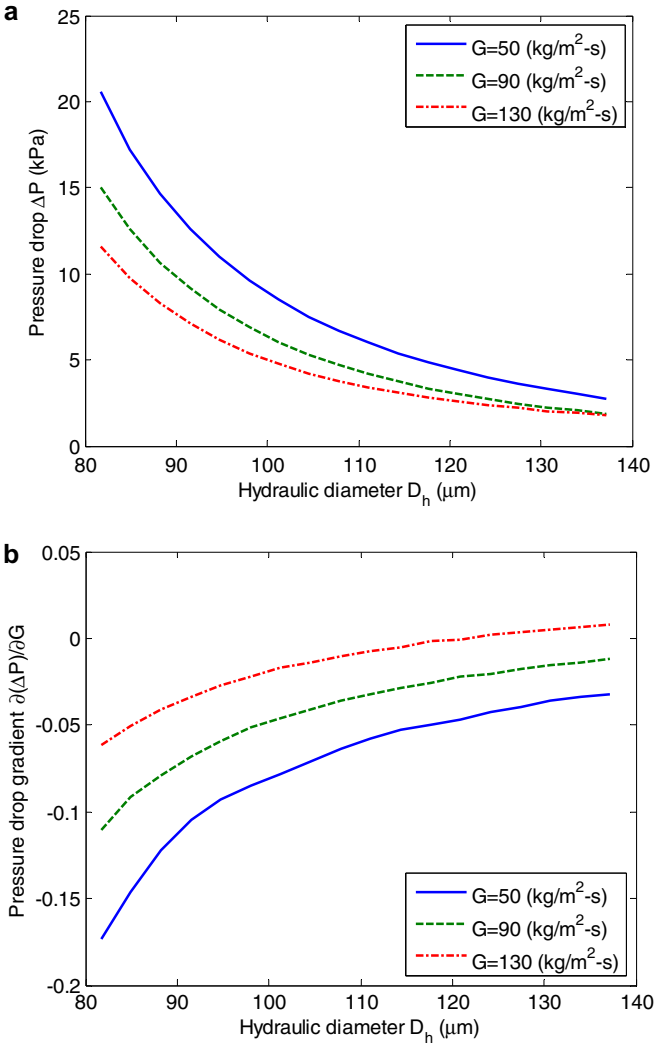

Fig. 16. The effect of channel hydraulic diameter at fixed pressure, heat flux and inlet subcooling on (a) pressure drop, and (b) pressure drop gradient under nominal conditions: $q'' \approx 44$ kW/m^2, $\Delta T_{sub} = 30$ °C, $P_{in} = 45$ kPa, $L = 15$ mm, water.

the overall heat transfer rate is a product of heat flux, channel length, and channel perimeter (p), $q = q'' \cdot L \cdot p$.

5.2. Inlet restriction effect

An inlet restrictor can be characterized by the following pressure drop model:

$$\Delta P_r = K_r \frac{\dot{m}^2}{\rho_{in} A_r^2} = K_r \frac{G_r^2}{\rho_{in}} \tag{19}$$

where ρ_{in} is the inlet density, $\dot{m}$ is the mass flow across the restrictor, and K_r is the discharge coefficient. The cross-sectional area of the inlet restrictor can be expressed as $A_r = \beta \cdot A$, where A is the overall cross-sectional area of the channel and $\beta \in [0, 1]$. It follows that the restrictor mass flux is $G_r = G/\beta$, where the channel mass flux is G. Usually, the inlet restrictor pressure drop is several times the channel pressure drop, and can also be expressed as $\Delta P_r = \gamma \cdot \Delta P_c$, where ΔP_c is the pressure drop from Eq. (13) between inlet pressure and exit pressure. Fig. 18 depicts the pressure drop of a channel with $\gamma = 8$ in comparison to a channel without an inlet restrictor. It is evident that the pressure drop–mass flux characteristic curves increases the flow stability by moving the mass flux at OFI and reducing the pressure drop–mass flux slope at mass fluxes lower than OFI compared to a channel with no inlet restrictor. This, of course, comes at the expense of higher pressure drops of the channel with inlet restrictors.

6. Conclusions

An experimental, numerical, and analytical study has been conducted to examine the Ledinegg instability in microchannels. The effects of system pressure, type of fluid, number of parallel channels, heat flux, inlet subcooling, and channel hydraulic diameter on flow instabilities were studied. The main conclusions are:

(1) System pressure is an important parameter controlling static flow instability: higher pressures will improve a flow boiling system's stability. This has important implications when using flow boiling of water for electronics cooling. Since a low saturation temperature is desired to enable boiling of water at low surface temperatures, water can only be considered for electronics cooling if operated at low pressures. The low reduced pressure required for these types of applications suggests that flow boiling instabilities will be a major problem if water is used.

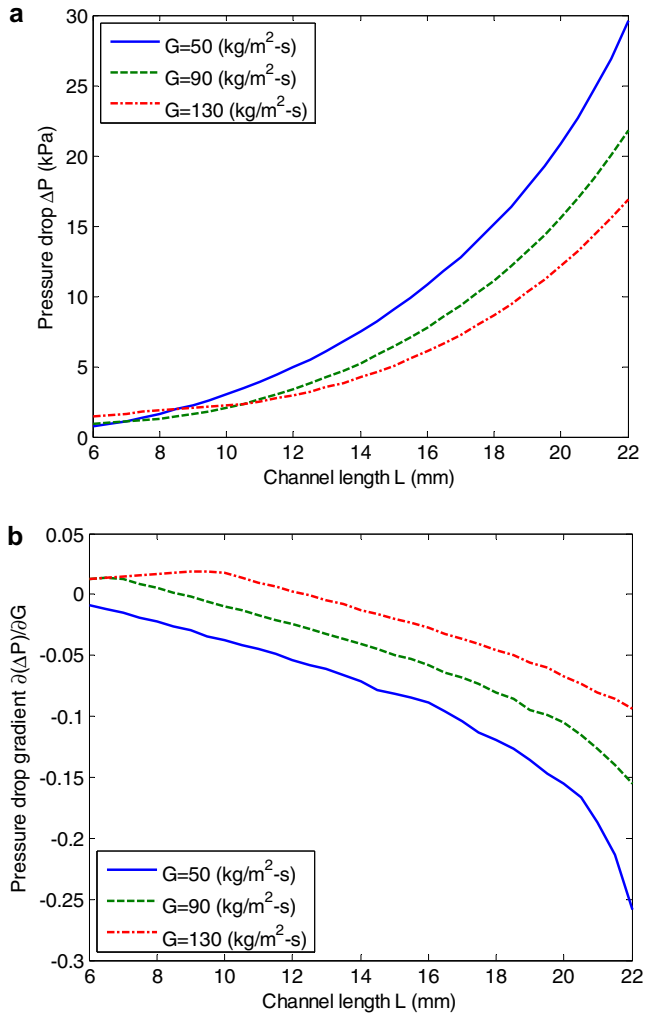

Fig. 17. The effect of channel length at fixed pressure and heat flux on (a) pressure drop and (b) pressure drop gradient under nominal conditions: $q'' \approx 44$ kW/m^2, $\Delta T_{sub} = 30$ °C, $P_{in} = 45$ kPa, $D_h = 100$ μm, water.

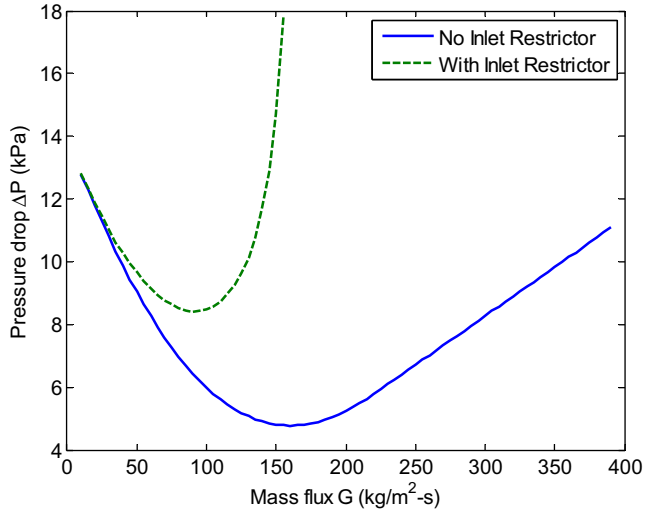

Fig. 18. The effect of inlet restriction on pressure drop–mass flux characteristics under nominal conditions; inlet restrictor pressure drop is 8 times of channel pressure drop. $q'' \approx 44$ kW/m^2, $\Delta T_{sub} = 30$ °C, $P_{in} = 45$ kPa, $D_h = 100$ μm, $L = 15$ mm, water.

(2) For cooling electronic equipment, the use of a coolant with a high reduced pressure (e.g., HFE-7100) can help alleviate static flow instabilities.
(3) Reducing the number of parallel channels improves the static stability of the flow.
(4) At low sub-atmospheric pressures, pressure drop in many applications can be a large fraction of the system pressure. Thus, for flow boiling, this can translate to a large variation in saturation temperature along the channel. For operating conditions that are pertinent to many low temperature applications, such as the ones investigated in this study, ignoring such a variation while using the Lockhart–Martinelli model will lead to large deviations from experimental results.
(5) The effects of heat flux, inlet temperature subcooling, and channel hydraulic diameter on the stability of the flow generally depend on the mass quality. For low mass qualities, near the onset of flow instability, reduced inlet subcooling, increased heat flux and reduced channel diameter tend to destabilize the flow. The opposite occurs at high mass qualities.

The Ledinegg instability is known as a static two-phase flow instability. It is usually coupled with other dynamic flow instabilities (e.g., the pressure-drop and density-wave instabilities). As mentioned in the above microchannel experimental observations, the pressure drop fluctuates greatly in the two-phase region, which is assumed to be the result of dynamic instabilities. In microchannels, the length/diameter ratio is usually much larger than that in conventional-scale channels, so the inherent compressibility in microchannel heat sinks is relatively greater; thus, self-sustained pressure-drop oscillations may be easily excited and observed. Quantitative modeling, analysis, and suppression of dynamic flow instabilities in microchannels are our next research endeavor.

Acknowledgements

The authors would like to thank the editor and reviewers for constructive comments. This work is supported by the Office of Naval Research (ONR) under the Multidisciplinary University Research Initiative (MURI) Award GG10919 entitled "System-Level Approach for Multi-Phase, Nanotechnology-Enhanced Cooling of High-Power Microelectronic Systems".

Appendix A

Consider the one-dimentional homogeneous momentum balance of a microchannel heat exchanger

$$\frac{\partial \dot{m}}{\partial t} + \frac{\partial (PA)}{\partial z} + \frac{1}{A}\frac{\partial}{\partial z}\left(\frac{\dot{m}^2}{\rho}\right) + F_{visc} = 0 \tag{20}$$

where the mass flow rate $\dot{m} = GA$, G is the mass flux and A is the cross-sectional flow area. By dividing A on both sides of (21), one may get

$$\frac{\partial G}{\partial t} = -\frac{\partial P}{\partial z} - \frac{\partial}{\partial z}\left(\frac{G^2}{\rho}\right) - F_{visc} \tag{21}$$

If the heat exchanger is assumed to be lumped along the flow path from 0 to L, then

$$\frac{dG}{dt} = \frac{P_{in} - P_{out}}{L} + \frac{1}{L}\left(\frac{G^2}{\rho_{in}} - \frac{G^2}{\rho_{out}}\right) - \frac{\Delta P_f}{L} = \frac{\Delta P_S - \Delta P_D}{L} \tag{22}$$

where $\Delta P_S = P_{in} - P_{out}$ is the external supply pressure drop, and the internal demand pressure drop ΔP_D includes both the accelerational and frictional pressure drops,

$$\Delta P_D = \Delta P_a + \Delta P_f, \quad \Delta P_a = \frac{G^2}{\rho_{out}} - \frac{G^2}{\rho_{in}}, \quad \Delta P_f = \int_0^L F_{visc}\, dz. \tag{23}$$

For boiling flow, $\rho_{out} < \rho_{in}$, so an accelerational pressure drop, $\Delta P_a > 0$, does exist; alternatively for the condensing flow, $\Delta P_a < 0$. For single-phase liquid flow, the fluid density changes only slightly, $\rho_{out} \approx \rho_{in}$, and, thus, the acceleration pressure drop is negligible.

Suppose that the lumped flow system (19) is maintained at an equilibrium mass flux G^*, then the linearized system with a small mass flux perturbation, δG, reads

$$L\frac{d(\delta G)}{dt} = \left[\frac{\partial(\Delta P_S)}{\partial G} - \frac{\partial(\Delta P_D)}{\partial G}\right] \cdot \delta G \tag{24}$$

Henec, it can be concluded that the flow system is unstable if $\frac{\partial(\Delta P_S)}{\partial G} \geqslant \frac{\partial(\Delta P_D)}{\partial G}$. A similar approach using the spatial momentum balance will result in the same conclusions.

For a microchannel heat exchanger, one-dimentional mass and energy balances can be used to characterize the fluid mass and heat transport,

$$\frac{\partial(\rho A)}{\partial t} + \frac{\partial \dot{m}}{\partial z} = 0 \tag{25}$$

$$\frac{\partial(\rho A u)}{\partial t} + \frac{\partial(\dot{m} h)}{\partial z} = \frac{q}{L} \tag{26}$$

where u is the specific internal energy, h the specific enthalpy, and q the heat input. In steady state, the mass flow rate is kept constant along the channel, then the energy balance equation (26) becomes

$$\frac{\partial h}{\partial z} = \frac{q}{\dot{m} L} = \frac{q'' \cdot S}{G \cdot A \cdot L} \tag{27}$$

where S and A are the surface and cross-sectional areas, respectively. Eq. (27) means that for constant heat flux q'', the local enthalpy change linearly with the channel flow path.

References

[1] S. Kakac, B. Bon, A review of two-phase flow dynamic instabilities in tube boiling systems, Int. J. Heat Mass Transfer 51 (2008) 399–433.
[2] M. Ozawa, H. Umekawa, K. Mishima, T. Hibiki, Y. Saito, CHF in oscillatory flow boiling channels, Inst. Chem. Eng. Symp. Ser. 79 (2001) 389–401.
[3] R.S. Daleas, A.E. Bergles, Effects of upstream compressibility on subcooled critical heat flux, ASME Paper No. 65-HT 67, ASME, New York, 1965.
[4] J.S. Maulbetsch, P. Griffith, A study of system-induced instabilities in forced-convection flows with subcooled boiling, MIT Engineering Projects Lab Report No. 5382-35, 1966.
[5] H.Y. Wu, P. Cheng, Visualization and measurements of periodic boiling in silicon microchannels, Int. J. Heat Mass Transfer 46 (17) (2003) 2603–2614.
[6] H.Y. Wu, P. Cheng, Boiling instability in parallel silicon microchannels at different heat flux, Int. J. Heat Mass Transfer 47 (2004) 3631–3641.
[7] A.E. Bergles, S.G. Kandlikar, On the nature of critical heat flux in microchannels, J. Heat Transfer 127 (2005) 101–107.
[8] L. Jiang, M. Wong, Y. Zohar, Phase change in microchannel heat sinks with integrated temperature sensors, J. Microelectromech. Syst. 8 (4) (1999) 358–365.
[9] L. Zhang, E.N. Wang, K.E. Goodson, T.W. Kenny, Phase change phenomena in silicon microchannels, Int. J. Heat Mass Transfer 40 (8) (2005) 1572–1582.
[10] A. Koşar, C.-J. Kuo, Y. Peles, Boiling heat transfer in rectangular microchannels with reentrant cavities, Int. J. Heat Mass Transfer 48 (23) (2005) 4867–4886.
[11] A. Koşar, C.-J. Kuo, Y. Peles, Suppression of boiling flow oscillations in parallel microchannels with inlet restrictors, J. Heat Transfer 128 (3) (2006) 251–260.
[12] M.E. Steinke, S.G. Kandlikar, An experimental investigation of flow boiling characteristics of water in parallel microchannels, J. Heat Transfer 126 (4) (2004) 518–526.
[13] C.-J. Kuo, Y. Peles, Flow boiling instabilities in microchannels and means for mitigation by reentrant cavities, J. Heat Transfer 130 (7) (2008) 072402.
[14] C.-J. Kuo, Y. Peles, Pressure effects on flow boiling instabilities in parallel microchannels, Int. J. Heat Mass Transfer 52 (1-2) (2009) 271–280.
[15] J.A. Bouré, A.E. Bergles, L.S. Tong, Review of two-phase flow instability, Nucl. Eng. Des. 25 (1973) 165–192.
[16] J.E. Kennedy, G.M. Roach, M.F. Dowling, S.I. Abdel-Khalik, S.M. Ghiaasiaan, S.S. Jeter, Z.H. Quershi, The onset of flow instability in uniformly heated horizontal microchannels, ASME J. Heat Transfer 122 (1) (2000) 118–125.
[17] R.S. Prasher, J. Dirner, J.-Y. Chang, A. Myers, D. Chau, D. He, S. Prstic, Nusselt number and friction factor of staggered arrays of low aspect ratio micro pin fins under cross flow for water as fluid, ASME J. Heat Transfer 129 (1) (2007) 141–153.
[18] 3M™ Novec™ Engineered Fluid HFE-7100.
[19] A. Bejan, A.D. Kraus, Heat Transfer Handbook, Ch. 5 Forced Convection: Internal Flows by A. Bejan; Ch. 9 Boiling by J.R. Thome, Wiley, New York, 2003.
[20] R.W. Lockhart, R.C. Martinelli, Proposed correlation of data for isothermal two-phase, two-component flow in pipes, Chem. Eng. Prog. 45 (1) (1949) 39–45.
[21] A. Kawahara, P. M.-Y. Chung, M. Kawaji, Investigation of two phase flow pattern, void fraction and pressure drop in a microchannel, Int. J. Multiphase Flow 28 (2002) 1411–1435.
[22] P. M.-Y. Chung, M. Kawaji, The effect of channel diameter on adiabatic two-phase flow characteristics in microchannels, Int. J. Multiphase Flow 30 (2004) 735–761.
[23] M. Kawaji, P.M.Y. Chung, Adiabatic gas–liquid flow in microchannels, Microscale Thermophys. Eng. 8 (2004) 239–257.
[24] S. Kandlikar, S. Garimella, D. Li, S. Colin, M.R. King, Heat Transfer and Fluid Flow in Minichannels and Microchannels, Elsevier, Amsterdam, 2005.
[25] J.G. Collier, J.R. Thome, Convective Boiling and Condensation, Oxford University Press, Oxford, 1996.
[26] V.P. Carey, Liquid–vapor phase-change phenomena: an introduction to the thermophysics of vaporization and condensation processes in heat transfer equipment, second ed., Taylor & Francis, New York, 2008.
[27] R.D. Flynn, D.W. Fogg, J.-M. Koo, et al., Boiling flow interaction between two parallel microchannels, ASME paper IMECE2006-14696, 2006.
[28] R. Stelling, E.V. McAssey, T. Dougherty, et al., The onset of flow instability for downward flow in vertical channels, ASME J. Heat Transfer 118 (3) (1996) 709–714.